Program Digest, 2019 IEEE International Ultrasonics Symposium (IUS)
Glasgow, Scotland, October 6-9, 2019

2-D Bayesian Displacement Estimation Improves Contrast-to-Noise/Resolution Trade-off in Shear Wave Elasticity Imaging

Thomas Ersepke, Tim C. Kranemann, and Georg Schmitz

Chair for Medical Engineering, Ruhr University Bochum, Bochum, Germany
{thomas.ersepke, tim.kranemann, georg.schmitz}@rub.de

***Abstract*—For time-of-flight reconstructions of shear wave speed (SWS) data, tissue displacements are typically tracked using windowed 1-D normalized cross correlation (NCC). The shear wave arrival times at laterally offset tracking positions are used for the reconstruction of the shear wave speed. Recent work has pointed out that one main source of error in SWS imaging is the uncertainty in the lateral tracking positions. Here, the tracking positions can be laterally shifted towards constructive interference of scatterers within the PSFs, used for the axial window during NCC estimation. Since the variance of the tracking position has a strong effect on the SWS estimates, large regression kernels and regularization are used, and a trade-off between an increased contrast-to-noise ratio (CNR) and a high lateral resolution is required. In this work, we present a novel Bayesian displacement estimation scheme incorporating RF data from a local 2-D neighborhood of uncorrelated speckle ensembles. The incorporation of a-priori knowledge from a 2-D neighborhood leads to a reduced variance of the tracking position and thus to an overall reduced variance of the shear wave arrival times. In simulation experiments, SWS images based on the proposed Bayesian estimator and the NCC estimator are compared with regard to the CNR and the resolution. The SWS images based on the proposed method yield an increase in CNR of up to twofold compared to the SWS images of the NCC estimation of similar resolution.**

***Index Terms*—Elastography, shear wave imaging, speckle, motion estimation, bayes methods**

I. Introduction

Shear wave elastography imaging (SWEI) is a clinically proven method for providing information on the tissue elasticity in addition to morphological ultrasound (US) data. Common SWEI methods use either phase-shift-based displacement estimators [1] or correlation-based estimators, e.g. the normalized cross correlation (NCC) estimator [2], to track the propagating shear wave. For many time-of-flight methods, the maximum displacement or maximum slope of displacement is detected at multiple tracking locations, and the differential arrival times as well as the distance of the tracking locations are used to calculate the shear wave speed, which is then related to the tissue stiffness [3].

With regard to system-dependent sources of error in SWEI, the accuracy of the displacement estimates can be limited by thermal noise, shearing-induced decorrelation [4] and finite tracking kernel lengths, bandwidth, and sampling rates [5] . These errors can therefore be assigned to features of the RF signals.

However, recent work has found that one main source of error in SWS imaging is the uncertainty in the tracking positions of the displacement estimates [6], [7], [8]. Here, the tracking positions can be laterally shifted towards constructive interference of scatterers within the PSFs, used for the axial window during displacement estimation. This position error leads to a delayed or early detection of the shear wave peak arrival time. Consequently, the measurements at inaccurate positions lead to a prolonged or shortened time delay measurement. Since inaccurate tracking positions have a strong effect on the SWS estimates, large regression kernels and additional regularization are used in SWEI reconstruction algorithms and a trade-off between an increased contrast-to-noise ratio (CNR) and a high lateral resolution is required [9].

In this work, we propose a novel displacement estimator, which is optimized with regard to the reduction of the tracking position error. The proposed method is based on the Bayesian displacement estimation framework in [10], where a-priori information is combined with the a correlation-based similarity metric of a centered estimate. For the proposed method, RF data from a local 2-D neighborhood of uncorrelated speckle ensembles is incorporated into the estimation. The incorporation of a-priori knowledge from a 2-D neighborhood leads to a reduced variance of the tracking position and thus to an overall reduced variance of the shear wave arrival times. The proposed 2-D Bayes estimator is compared to the standard NCC estimator using numerical simulations. For the reconstruction of the SWS data, the multi-resolution method [9] is employed. The resulting SWS images are investigated with regard to their CNR and resolution.

II. Methods

A. 2-D Bayes Displacement Estimator

For the estimation of the axial displacement, two axial segments of RF data are defined

$$s_1(n+k) = s(x_i,\, z_k\,, t_1), \quad n \in \left[{}^{-N}\!/2, {}^{+N}\!/2\right], \qquad (1)$$

This work was funded by the German Federal Ministry of Education and Research, contract number 13GW0069A-B (project SAMBA-PATI).

$$s_l(n+k) = s(x_i,\, z_k\,, t_l), \quad n \in [-{}^{N}\!/2,\, +{}^{N}\!/2],\, l \in [2, L]\,, \tag{2}$$

where s_1 is an axial segment of an RF line in a reference frame at time t_1 and s_l is a segment of an RF line in a later frame at time t_l after the displacement of the scatterers. Both signal segments s_1 and s_l have the same lateral position x_i. The segments s_1 and s_l are centered around the same axial position z_k with equal segment length N.

In general, the Bayes theorem for the estimation of the displacement at the axial location k can be written as

$$p_{k,i}(u|s_1, s_l) = \frac{p_{k,i}(s_1, s_l|u)\, p_{\mathcal{T}_{k,i}}(u)}{\int p_{k,i}(s_1, s_l|u)\, p_{\mathcal{T}_{k,i}}(u)\, \mathrm{d}u} \tag{3}$$

where $p_{k,i}(u|s_1, s_l)$ is the posterior probability density function (PDF). The posterior PDF is combined by the current information $p_{k,i}(s_1, s_l|u)$, which resembles a similarity metric of $s_1(n)$ and $s_l(n)$, and the prior information $p_{\mathcal{T}_{k,i}}(u)$. In contrast to [10], [11], this prior information is obtained from segments in a local, 2-D neighborhood $\mathcal{T}_{k,i}$. The denominator in (3) scales the posterior PDF. Because only the argument which maximizes $p_{k,i}(u|s_1, s_l)$ is of interest, (3) can be rewritten in the log-domain

$$\ln(p_{k,i}(u|s_1, s_l)) \propto \ln(p_{k,i}(s_1, s_l|u)) + \ln(p_{\mathcal{T}_{k,i}}(u)). \tag{4}$$

According to [10], the similarity metric is formulated as a sum of squared differences (SSD)

$$\ln(p_{k,i}(s_1, s_l|u')) = \\ -\frac{1}{4\sigma^2_{\mathrm{noise},k,i}} \sum_{m=-N/2}^{N/2} (s_1(m+k) - s_l(m+k-\widehat{u}_{\mathrm{in},k,i}-u'))^2 \tag{5}$$

where $s_l(n - \widehat{u}_{\mathrm{in},k,i})$ was already undelayed towards $s_1(n)$ by an initial estimate $\widehat{u}_{\mathrm{in},k,i}$ to reduce the search region of (5) and u' is the residual displacement. The estimated noise power $\sigma^2_{\mathrm{noise},k,i}$ describes the amount of uncertainty and weights $\ln(p_{k,i}(s_1, s_l|u'))$ with regard to (4). It is derived using a peak correlation coefficient approach for estimating the local SNR $\widehat{\eta}_{\mathrm{SNR},k,i}$ at location $(x_i, z_k)^{\mathsf{T}}$ [10]

$$\widehat{\eta}_{\mathrm{SNR},k,i} = \frac{\rho_{k,i}}{1-\rho_{k,i}}\,, \tag{6}$$

where $\rho_{k,i}$ is the peak correlation coefficient of the normalized cross correlation between $s_1(n)$ and $s_l(n)$. Then, $\sigma^2_{\mathrm{noise},k,i}$ is

$$\sigma^2_{\mathrm{noise},k,i} = \frac{\sigma^2_{\mathrm{RF},k,i}}{\widehat{\eta}_{\mathrm{SNR},k,i}+1} \tag{7}$$

where $\sigma^2_{\mathrm{RF},k,i}$ is the power of the RF data and is estimated by calculating the geometric mean of the two signal powers of $s_1(n)$ and $s_l(n)$ [10].

We propose to use a-priori information from a ring of neighboring estimates, consisting of the two direct axial neighboring estimates (AN), two direct lateral neighboring estimates (LN) and the 4 diagonal neighboring estimates (DN). Fig. 1 depicts the estimates from the 2-D neighborhood representing the a-priori information. The weights are determined according to the distance of the neighboring segments to the center segment. With an increased distance to the center segment, it is assumed that the value of additional information for the estimation is decreasing. The total distance used for scaling the weights to $\sum_{\mathrm{j}\in\mathcal{T}_{k,i}} w_{\mathrm{j}} = 1$ is given by

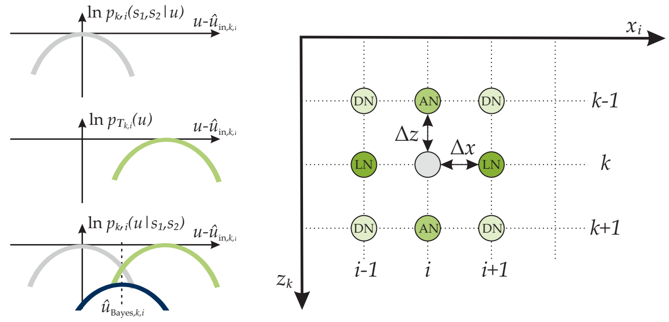

(a) (b)

Figure 1: Workflow of the Bayesian displacement estimation: (a) $\ln(p_{k,i}(s_1, s_l|u))$ and $\ln(p_{\mathcal{T}_{\mathrm{k,i}}}(u))$ are combined in (4). (b) 2-D neighborhood of initial estimates. The weight of the initial estimates is determined by the euclidean distance of the particular segments to the center segment.

$$d_{tot} = 2\Delta z + 2\Delta x + 4\sqrt{(\Delta x)^2 + (\Delta z)^2}\,. \tag{8}$$

where Δz is the axial discretization of the NCC estimates (depending on N and the overlap). Further, Δx is the lateral discretization of the RF data and hence the lateral discretization of the NCC estimates. With the total distance, the particular weights of the AN, LN and DN are calculated by $w_{AN} = \Delta z/d_{tot}$, $w_{LN} = \Delta x/d_{tot}$, $w_{DN} = \sqrt{(\Delta x)^2 + (\Delta z)^2}/d_{tot}$. When the center segment was located at one side or in one corner of the region of interest, the weights of the missing neighboring estimates were set to zero and d_{tot} was calculated based on the remaining weights.

The prior information $p_{\mathcal{T}_{k,i}}(u')$ is incorporated in the manner of a generalized Gaussian-Markov random field

$$\ln(p_{\mathcal{T}_{k,i}}(u')) = -\frac{1}{p\lambda_B^p} \sum_{\mathrm{j}\in\mathcal{T}_{k,i}} w_{\mathrm{j}} |\widehat{u}_{\mathrm{j}} - \widehat{u}_{\mathrm{in},k,i} - u'|^p\,, \tag{9}$$

where $\widehat{u}_{\mathrm{j}}$ are initial displacement estimates located within the neighborhood $\mathcal{T}_{k,i}$. As in (5), those estimates are already undelayed by $\widehat{u}_{\mathrm{in},k,i}$. The parameter p specifies the shape of the prior distribution $\ln(p_{\mathcal{T}_{k,i}}(u'))$ with $p \in [1; 2]$. For $p = 2$, the prior PDF equals a Gaussian distribution, where discontinuities in displacements between segments are stronger penalized. The parameter λ_B is the main weighting parameter which determines how strongly $\ln(p_{k,i}(u|s_1, s_l))$ is influenced by the prior PDF.

The estimate $\widehat{u}_{\mathrm{Bayes},k,i}$ is found through updating $\widehat{u}_{\mathrm{in},k,i}$ by the residual displacement which maximizes the posterior PDF $\ln(p_{k,i}(u'|s_1, s_l))$

Table I: US SIMULATION PARAMETERS

Parameter	Value/ Range
Center frequency f_c	7.8 MHz
Bandwidth (-6dB)	101.5 %
Sampling frequency f_s	1 GHz
Speed of sound c	1540 m/s
Probe focus	25 mm
Attenuation	none
Element width	180 μm
Element pitch	200 μm
Sampling period Δt	200 μs
SNR of RF data η_{SNR}	20dB, $+\infty$

$$\widehat{u}_{\mathrm{Bayes},k,i} = \underset{u'}{\operatorname{argmax}}(\ln(p_{k,i}(u'|s_1, s_l))) + \widehat{u}_{\mathrm{in},k,i}\,. \qquad (10)$$

After updating the posterior PDF in (10), $\widehat{u}_{\mathrm{Bayes},k,i}$ is saved as new initial estimation $\widehat{u}_{\mathrm{in},k,i}$ and the algorithm is executed for the next iteration. For the 2-D Bayes estimator, a fixed number of iterations $N_{\mathrm{it}} = 5$ was used and the two Bayes parameters were set to $\lambda_B = 8 \cdot 10^{-9}\,\mathrm{m}$ and $p = 2$.

B. Numerical Simulations

In order to validate the feasibility of the proposed estimator for SWS imaging, simulations of plane shear waves were realized by solving the 1-D linearized shear wave differential equation numerically. Therefore, a finite differences time domain (FDTD) method was implemented in MATLAB. For the simulations of a 2-D plane shear wave, the 1-D wave simulation was extended in the z-direction.

For the shear wave excitation, the initial displacement function was chosen to resemble a typical shear wave in elastography applications. The center frequency was chosen to $350\,\mathrm{Hz}$ and the bandwidth was chosen to $200\,\%$. The displacement magnitude was set to 10 μm. Two homogeneous SWS regions with $c_{low} = 2.2\,\mathrm{m/s}$ and $c_{high} = 5\,\mathrm{m/s}$, separated by a vertical boundary, were simulated.

The US simulations were performed using the US simulation toolbox Field II [12]. Walking aperture beamforming was used in this simulation. For each line of RF data, a subaperture, centered around that RF line, was used. A summary of the simulation parameters is given in Tab. I.

A number of 35 scatterers per resolution cell was used for the simulation, while it has been shown that 11 scatterers per resolution cell are already sufficient to achieve full speckle statistics [13]. The RF signal sampling frequency f_s was set to $1\,\mathrm{GHz}$. The first frame of US data was simulated with the initial spatial distribution of scatterers. Thereafter, the scatterer positions were displaced by the simulated shear wave field. Subsequent US frames were simulated with a sampling period of $\Delta t = 200\,\mu\mathrm{s}$. White Gaussian noise of varying noise powers was added to the simulated data leading to varying signal-to-noise ratios (SNRs) η_{SNR} of the acquired RF data.

C. Displacement Estimation

As reference method, 1-D windowed NCC [14] was used. As proposed in [14], sub-sample accuracy is achieved in two stages in this work. First, the acquired RF data is up-sampled using Fourier-domain interpolation. Secondly, a parabolic fit to the peak of the cross-correlation function is performed and the argument, which maximizes the function is derived algebraically.

The segment length N of the NCC and the 2-D Bayes estimator was set to 2.5λ and the relative segment overlap to 75% leading to $\Delta z = 0.625\lambda$. The lateral discretization of the RF data was $\Delta x = 200\,\mu\mathrm{m}$. The 2-D Bayes estimator was implemented as described in II-A.

D. Shear Wave Speed Reconstruction

For the reconstruction of the SWS data $\widehat{c}$, the multiresolution approach by Hollender et al. [9] was employed. Here, the time delays are measured between all combinations of locations within a kernel of size K. The time-of-flight problem is presented as an overdetermined system of linear equations that can be directly solved using the least-squares solution. Spatial constraints on the multiresolution solution are imposed by Tikhonov regularization, weighted by λ_Γ, for additional noise suppression at the expense of lateral resolution.

E. Quality Metrics

To calculate the contrast-to-noise ratio (CNR) of the SWS estimates, the mean values $\bar{c}_{high}$, $\bar{c}_{low}$ of the SWS estimates $\widehat{c}$ as well as the variances of the estimates σ^2_{high}, σ^2_{low} were determined on each side of the vertical boundary. The CNR was computed as

$$r_{\mathrm{CNR}} = \frac{|\bar{c}_{high} - \bar{c}_{low}|}{\sqrt{\sigma^2_{high} + \sigma^2_{low}}}\,. \qquad (11)$$

To determine the lateral resolution, the width of the vertical boundary was measured. Therefore, the mean SWS was calculated along each column. Then, the intercepts of the mean SWS profile with the constants $\bar{c}_{high}$ and $\bar{c}_{low}$ were determined, which were closest to the location of the boundary. The resolution was determined as the distance between the two intercepts.

III. RESULTS

Fig. 2 shows the SWS reconstruction results for both displacement estimators. For the reconstruction, the kernel size was set to $K = 3$ and the regularization was set to $\lambda_\Gamma = 10$. It can be seen that areas of homogeneous SWS appear much more noisy for the NCC result, compared to the Bayes result. At the same time, the vertical boundary of the Bayes result is not significantly more blurred than the boundary of the NCC result. Fig. 3 shows the CNR/resolution trade-off, with regard to the SWS images based on the two displacement estimation schemes. In Fig. 3.a, the results of the simulations without added noise ($\eta_{\mathrm{SNR}} = +\infty$) are depicted. Here, λ_Γ was set to

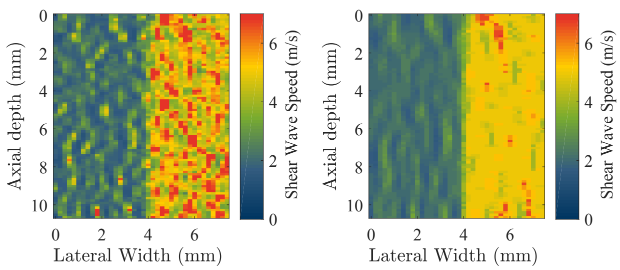

(a) NCC result, $K = 3$, $\lambda_\Gamma = 10$

(b) Bayes result, $K = 3$, $\lambda_\Gamma = 10$

Figure 2: Reconstructed SWS images for the SWEI simulations without added RF data noise ($\eta_{\text{SNR}} = +\infty$). The SWS reconstruction parameters were set to $K = 3$ and $\lambda_\Gamma = 10$. (a) NCC displacement estimation applied prior to reconstruction, (b) Bayes displacement estimation applied prior to reconstruction.

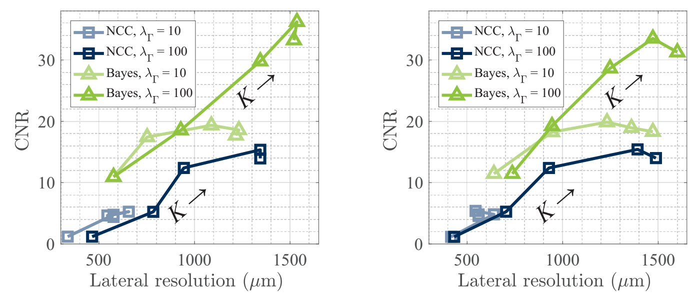

(a) $\eta_{\text{SNR}} = +\infty$

(b) $\eta_{\text{SNR}} = 15\,\text{dB}$

Figure 3: Contrast-to-noise ratio and resolution trade-off curves for both estimation schemes. The kernel size K and regularization parameter λ_Γ were varied, leading to varying CNR and resolution values. The Bayes results (green triangles) show an improved CNR compared to the NCC results (blue squares) of similar resolution.

10 and 100, respectively, and the kernel size was varied leading to varying CNR and resolution values. For both regularization settings, the Bayes results showed an improved trade-off between the CNR and the resolution. This becomes evident for the NCC result with a resolution of $900\,\mu\text{m}$ and a CNR of 12. Here, the corresponding Bayes results showed either an increased CNR (19) and comparable resolution or an improved resolution $(550\,\mu\text{m})$ and comparable CNR.

These findings are further confirmed, when noise was added to the simulated RF data. In Fig. 3.b, the NCC and the Bayes results are shown for $\eta_{\text{SNR}} = 15\,\text{dB}$. Similar to Fig. 3.a, the Bayes results outperformed the NCC results, with regard to the CNR/resolution ratio of the SWS images. In comparison to results without RF data noise, the resolution of the SWS images was slightly decreased for both estimators.

IV. Conclusions

In SWEI, inaccurate positions displacement estimates caused by the speckle effect have a major impact on the quality of SWS images [6], [7]. For the optimization of displacement estimation algorithms with regard to the applicability for SWEI, this circumstance needs to be taken into account.

We proposed a novel Bayesian displacement estimator where a-priori information from a local 2-D neighborhood is incorporated. By using this information from uncorrelated speckle ensembles, the position error could be reduced. This was confirmed by the results in the simulation experiments with and without added RF data noise. Compared to the conventional NCC estimation, the proposed displacement estimation, leads to SWS images with an overall increased CNR/resolution trade-off and a gain in CNR up to the factor of 2 compared to the NCC results of similar resolution.

References

[1] T. Loupas, J. Powers, and R. W. Gill, "An axial velocity estimator for ultrasound blood flow imaging, based on a full evaluation of the doppler equation by means of a two-dimensional autocorrelation approach," *IEEE Trans. Ultrason., Ferroelectr., Freq. Control*, vol. 42, no. 4, pp. 672–688, 1995.

[2] O. Bonnefous, P. Pesqué, and X. Bernard, "A new velocity estimator for color flow mapping," in *Proc. IEEE Ultrason. Symp*, 1986, pp. 855–860.

[3] M. L. Palmeri, M. H. Wang, J. J. Dahl, K. D. Frinkley, and K. R. Nightingale, "Quantifying hepatic shear modulus in vivo using acoustic radiation force," *Ultrasound Med. Biol.*, vol. 34, no. 4, pp. 546–558, 2008.

[4] I. Céspedes, C. de Korte, and A. van der Steen, "Echo decorrelation from displacement gradients in elasticity and velocity estimation," *IEEE Trans. Ultrason., Ferroelectr., Freq. Control*, vol. 46, no. 4, pp. 791–801, 1999.

[5] W. F. Walker and G. E. Trahey, "A fundamental limit on delay estimation using partially correlated speckle signals," *IEEE Trans. Ultrason., Ferroelectr., Freq. Control*, vol. 42, no. 2, pp. 301–308, 1995.

[6] S. A. McAleavey, L. O. Osapoetra, and J. Langdon, "Shear wave arrival time estimates correlate with local speckle pattern," *IEEE Trans. Ultrason., Ferroelectr., Freq. Control*, vol. 62, no. 12, pp. 2054–2067, 2015.

[7] P. J. Hollender, S. J. Rosenzweig, K. R. Nightingale, and G. E. Trahey, "Single-and multiple-track-location shear wave and acoustic radiation force impulse imaging: matched comparison of contrast, contrast-to-noise ratio and resolution," *Ultrasound Med. Biol.*, vol. 41, no. 4, pp. 1043–1057, 2015.

[8] T. Ersepke, T. C. Kranemann, and G. Schmitz, "Quantification of noise in shear wave elasticity imaging caused by speckle," in *Proc. IEEE Int. Ultrason. Symp. (IUS)*, 2019.

[9] P. Hollender, N. Bottenus, and G. Trahey, "A multiresolution approach to shear wave image reconstruction," *IEEE Trans. Ultrason., Ferroelectr., Freq. Control*, vol. 62, no. 8, pp. 1429–1439, 2015.

[10] D. Dumont and B. Byram, "Robust tracking of small displacements with a bayesian estimator," *IEEE Trans. Ultrason., Ferroelectr., Freq. Control*, vol. 63, no. 1, pp. 20–34, 2016.

[11] T. Ersepke, T. C. Kranemann, and G. Schmitz, "On the performance of time domain displacement estimators for magnetomotive ultrasound imaging," *IEEE Trans. Ultrason., Ferroelectr., Freq. Control*, vol. 66, no. 5, pp. 911–921, 2019.

[12] J. A. Jensen, "Field: A program for simulating ultrasound systems," in *Med. Biol. Eng. Comput.*, vol. 34, suppl. 1, pt. 1, 1996, pp. 351–353.

[13] M. L. Palmeri, S. A. McAleavey, G. E. Trahey, and K. R. Nightingale, "Ultrasonic tracking of acoustic radiation force-induced displacements in homogeneous media," *IEEE Trans. Ultrason., Ferroelectr., Freq. Control*, vol. 53, no. 7, pp. 1300–1313, 2006.

[14] G. F. Pinton, J. J. Dahl, and G. E. Trahey, "Rapid tracking of small displacements with ultrasound," *IEEE Trans. Ultrason., Ferroelectr., Freq. Control*, vol. 53, no. 6, pp. 1103–1117, 2006.